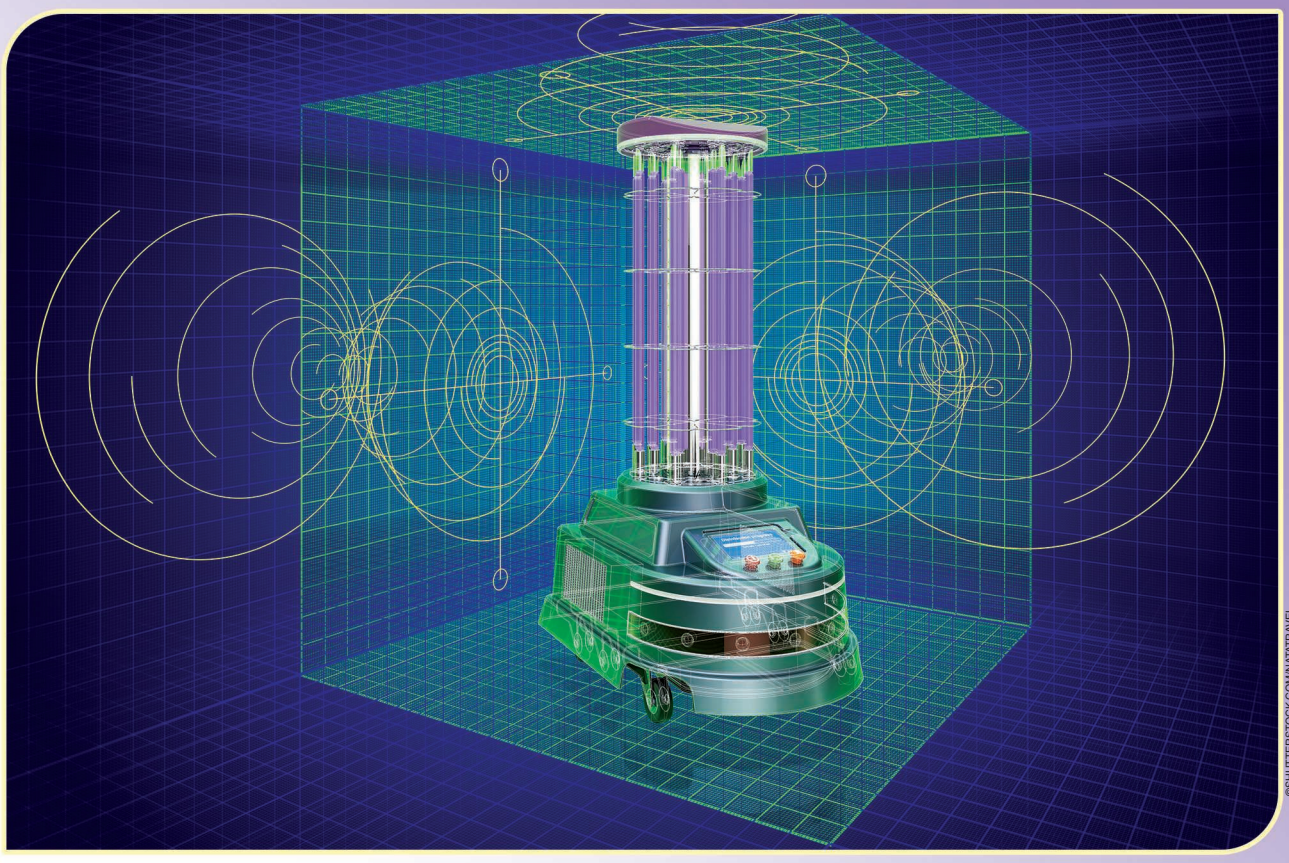

©SHUTTERSTOCK.COM/NATATRAVEL

UV-C Mobile Robots With Optimized Path Planning

Algorithm Design and On-Field Measurements to Improve Surface Disinfection Against SARS-CoV-2

By Luca Tiseni, Domenico Chiaradia, Massimiliano Gabardi, Massimiliano Solazzi, Daniele Leonardis, and Antonio Frisoli

Digital Object Identifier 10.1109/MRA.2020.3045069
Date of current version: 25 January 2021

Ultraviolet type-C irradiation (UV-C) is an effective no-contact disinfection procedure for surfaces and environments to reduce the spread of severe acute respiratory syndrome coronavirus 2 (SARS-CoV-2), the virus that causes COVID-19. This work evaluates the effect of the adoption of mobile robots for UV-C irradiation, compared to conventional disinfection methods based on static UV-C lamps. On-field evaluation was conducted to measure the energy dose delivered by a robot-based moving source of UV-C radiation at different locations in an indoor environment. The effectively released radiation dose was experimentally measured using distributed UV-C-sensitive detectors, considering all of the environmental factors involved. Moreover, this article proposes a novel trajectory planner

consisting of a genetic algorithm (GA) that explores the possible trajectories and disinfection outcomes of a robot moving in a tunable artificial potential field (APF) and is capable of maximizing the delivered UV dose based on ambient geometry. The experimental results show that, compared to a conventional trajectory, an optimized one has better performance in terms of both the coverage of the radiated energy in the environment and the time required to complete the disinfection task.

Robotic Technology and UV-C Radiation

The SARS-CoV-2 outbreak poses novel challenges and constraints to our everyday life, particularly in terms of concerns about safe access to public spaces, shared environments, and workplaces. As outlined in [1]–[3], robotic solutions, together with artificial intelligence and automation, can be effectively used for disinfection, delivering medications or food, and performing remote diagnosis, thus limiting the risk of human operators' exposure to potentially contaminated environments. Regarding the disinfection of environments and surfaces, there are different contactless solutions [4]. UV-C irradiation is known to be very successful for virus inactivation and bacteria disinfection by reducing contamination on high-touch surfaces [5]–[7]. UV-C irradiation can also be particularly effective against SARS-CoV-2. In this context, disinfection procedures with UV-C irradiation having a wavelength in the range of 200–280 nm are the most efficient since UV-C photons are absorbed by viruses at the level of nucleic acid bases. The scientific literature has already observed and quantified the virucidal effect of UV-C irradiation against SARS-CoV-2. In particular, a recent study has demonstrated how both replication inhibition and inactivation are achieved as a function of delivering equivalent doses of UV-C to 3.7 mJ/cm^2 for reaching a 3-log reduction of the viral concentration and up to 16.9 mJ/cm^2 to achieve a complete virus inhibition [8].

UV-C irradiation is known to be very successful for virus inactivation and bacteria disinfection by reducing contamination on high-touch surfaces.

Figure 1. The experimental setting involving a UV-C-equipped mobile robot in a conference room at the Scuola Superiore Sant'Anna of Pisa.

The evolution of robotic technology combined with UV-C irradiation systems demonstrates a significant advantage compared to fixed UV-C-radiation sources. UV-C-radiation technology combined with autonomous robotic systems has been successfully adopted in both scientific studies [9], [10] and commercially available products [Model C (UVD Robots, www.uvd-robots.com/robots); PHS-M mobile robot (Klainrobotics, www.phs-uv.com/phs-m/); TMiRob (TMI Medical, www.tmirob.com/solutions/19)]. Fixed UV-C sources are not capable of guaranteeing equivalent levels of UV-C doses at different distances from the source; in fact, the administered dose of UV radiation is a function of both the intensity of irradiation and exposure time. To date, most of the existing studies refer only to systems with a fixed positioning of the emitting UV-radiation source. To our knowledge, there are no previous works analyzing how the use of a mobile source of radiation can be optimized according to the geometrical properties of the environment to provide a sufficient radiation dose on all surfaces.

In this article, we experiment with the efficacy of UV robots for surface and environment disinfection, and we investigate how the robot path can be optimized to reach the maximum UV-irradiation performance based on environmental geometry. In detail, this article presents the development of a new robotic autonomous system for the contactless ambient disinfection of air and surfaces via UV-C irradiation and a novel genetic-optimization algorithm for robot-motion planning (see Figure 1 for a view of the system). On the basis of a physical irradiation model, it can optimize the delivered UV-C-radiation dose as a function of the geometric properties of the environment. Further, the experimental assessment of the disinfection efficacy of the robot was evaluated in two experiments. In the first, we performed a comparison of the effectiveness of a static versus mobile source of radiation in a real indoor environment. In the second, we evaluated the performance of the optimized robot-motion path generated by the proposed novel algorithm compared to a standard path.

System Description

The components of the developed robot are indicated in Figure 2(a) while the architecture of the overall robotic system is depicted in Figure 2(b). The upper part of the robot hosts the UV-C system consisting of four lamps, 0.8 m long, mounted at a height of 0.48 m from the ground, each with a nominal power of 75 W and a UV-C-radiation efficient power of 20 W (Sterilsan). In more detail, the lamps are low-pressure, mercury-vapor-based discharge lamps that emit light in the UV-C

band, with a 254-nm wavelength peak emission. The high-level control for a remote and autonomous condition hosts a Robot Operating System with a version of real-time appearance-based mapping (RTAB-Map) [11] to obtain localization of the robot in the environment and to eventually perform simultaneous localization and mapping (SLAM). SLAM is used to perform an initial, supervised mapping of the area of operation, whereas, in the repeated use of the robot as a disinfection system, localization is envisaged to be enabled only to increase the robustness of the system. The implemented RTAB-Map parametrization makes use of red, green, blue depth (RGB-D) data, lidar, and wheel-odometry data, and it is constrained to planar localization and mapping. A 2D occupancy grid is generated through the lidar sensor.

Experimental Evaluation of the Efficacy of a Static Versus Mobile Source of UV-C Radiation

The first objective of this study was to investigate the efficacy of robot-carried sources of UV-C radiation compared to fixed-lamp solutions. In our study, we used low-pressure mercury lamps (254 nm). The disinfection efficacy of single-source UV irradiation has been widely studied in scientific literature, especially against *Clostridium difficile* bacterium [12]. Moreover, the dependency of the disinfection performance on the radiation dose has been studied in [13], including the strong influence of both irradiation time and irradiated energy on the reduction of bacteria concentration. The aim of the experiment was to assess whether, during a room-disinfection task, a robotic solution can perform better than a fixed-lamp solution in terms of irradiation time and irradiated energy distribution.

Methods

To experimentally measure the differences between a fixed UV-C-emitting device and a mobile one, a disinfection task was performed in a conference room at the Scuola Superiore Sant'Anna of Pisa, measuring about 60 m^2. Twenty-one colorimetric UV-sensitive markers (Intellego) were placed at

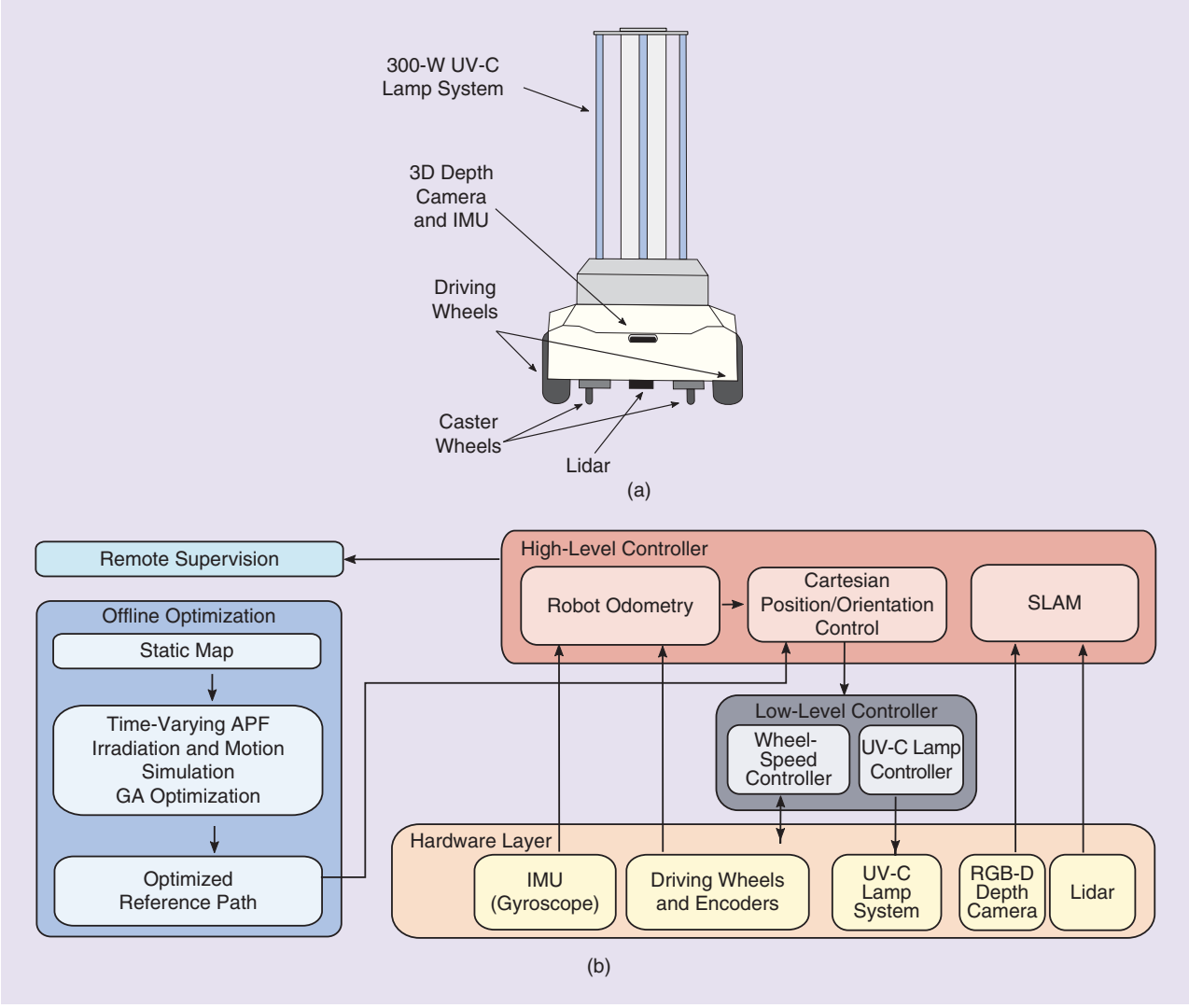

Figure 2. A schematic view of (a) the robotic mobile platform and (b) the control architecture. The arrows indicate the data/command stream direction and the relation among hardware/software components. IMU: inertial measurement unit.

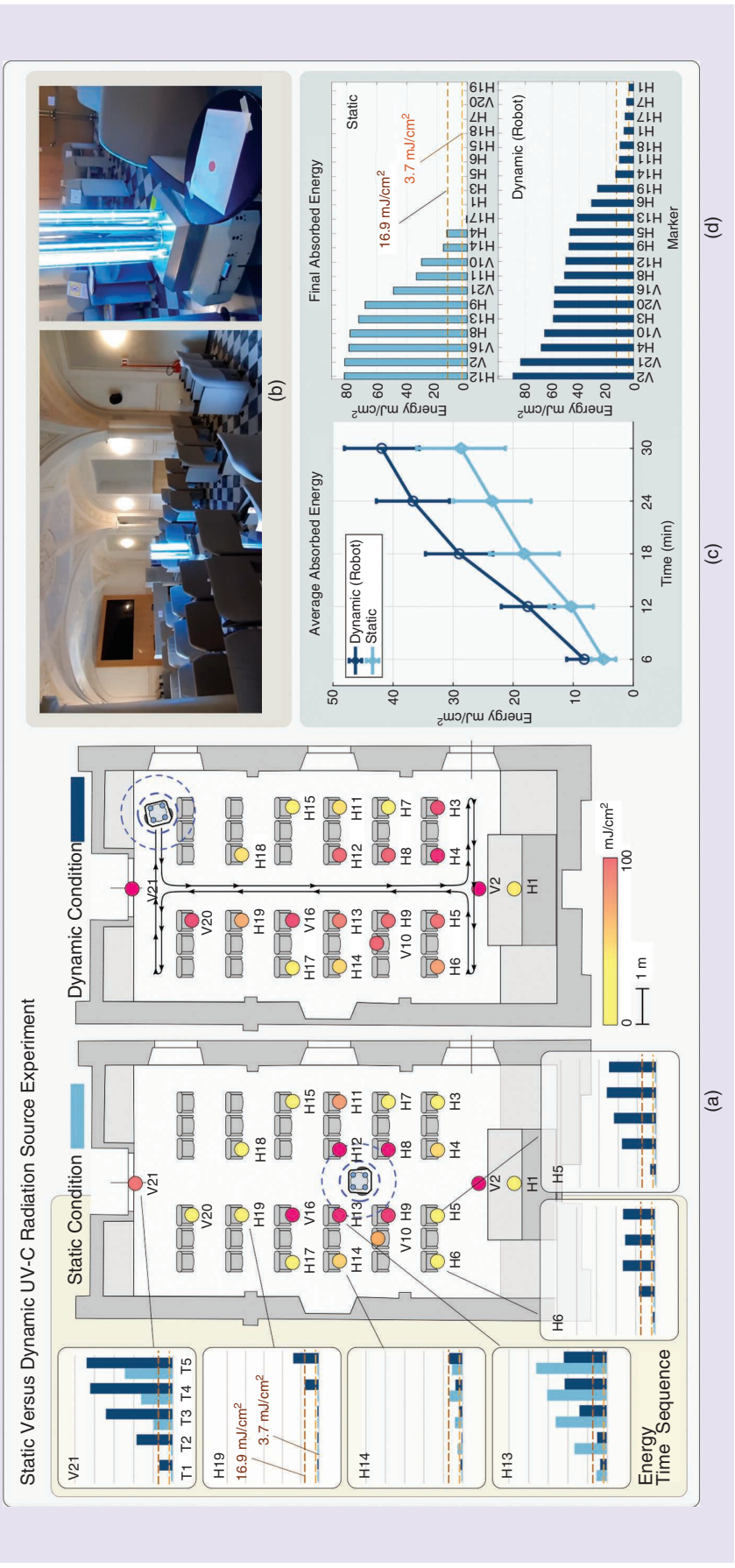

Figure 3. The results of the experimental comparison between the static and dynamic sources of UV-C radiation. (a) The result maps of the two conditions. In the static condition, the robot is fixed at the center of the room; in the dynamic, it moves along the reported trajectory (black line). The marker's code starts with "H" if it is horizontal (e.g., if it lies on the chair) or with "V" if it is vertical (e.g., it is attached to the door). (b) Some pictures of the experimental setup and (c) a comparison of the average absorbed energy over time in the two conditions. (d) The bar plots of the final absorbed energy for each marker.

different locations and orientations in the room according to the map presented in Figure 3. In the room, there was a table and a set of six rows of chairs with a central corridor. The robot could move along the central corridor and behind the first and last rows of chairs. The markers were placed on the table (H1) and its lateral side (V2), both vertically and horizontally oriented (from H3 to H20) on the chairs, and on the entrance door (V21). The room was then exposed to UV irradiation in two different conditions: 1) static: UV irradiation with a fixed position of the lamp, located at the center of the room; and 2) dynamic: UV irradiation from a mobile lamp mounted on the robot, moving continuously along a predetermined path. The robot was remotely guided at a constant speed (0.2 m/s) by a human operator provided with visual feedback from the robot camera. Energy data was calculated by acquiring the markers' colors through a digital scanner (Kyocera TaskAlfa 3551ci) and extracting their RGB values. According to the reference chart in Figure 4, we used the green (G) channel to calculate the energy value for each marker, based on a least-squares linear fit of the available colors. The relation used is $E = mG + q$, where E is the energy, G is the marker's color green value, and the coefficients are $m = -0.769$ and $q = 182.7$. The experimental design was a two-way (2 × 5), repeated

measures analysis of variance (ANOVA) design study with two factors: irradiation condition (robot versus static for a total time of 30 min) and time (five levels with color sampling performed every 6 min).

Results

Figure 3 reports the distribution of irradiation at the end of the experiment in the room. After 30 min of exposure, log-3 SARS-CoV-2 virus inactivation values (3.7 mJ/cm^2 [8]) were reached by 100% of the samples in the dynamic condition and by only 52.38% of the samples (11/21) in the static condition (Fisher exact test, $p = 0.0005$). The F-statistics associated with the two-way ANOVA experimental design revealed a significant effect for both factor time ($F(1,4) = 33.51$, ($p < 1e^{-5}$) and the interaction factor "time × experimental condition" ($F(1,4) = 2.876$, $p = 0.028$). Moreover, a difference in the treatment condition was obtained, although still nonstatistically significant, at 0.05 level ($F(1,4) = 3.455$, $p = 0.078$). The results clearly indicate that there is an interaction between time and experimental condition; the exposure to radiation was strictly dependent on time in the static condition (linear relation of released energy), and, when the robot worked near the static source location, its effect on the markers' irradiation was close to the effect of the static source.

Differences in the absorbed energy of nearby markers, especially in the static condition, evidence the effect of object shadowing (i.e., chair armrests and backseats) and of the different surface orientations. The contribution of indirect radiation by light diffusion appears negligible in the explored exposition time. Figure 3 (c) displays the mean value of the delivered UV-C irradiation energy over time (the "Average Absorbed Energy" graph), computed as the mean of all detectors at each time, with higher values of irradiation delivered in the dynamic condition compared to the static one. As illustrated in Table 1, at 24 min a significant difference in delivered irradiation energy (paired t-test $p < 0.05$) was reached, with almost the same level kept at 30 min. In fact, if the robot works mostly in proximity of the static lamp's position during a time interval, the mean difference remains almost the same, as the two conditions overlap considerably.

In this experiment, the two limit conditions of a static source of radiation compared to a continuously moving one were tested. However, in a real application of a static UV-C lamp, a human operator could manually reposition a fixed radiation source several times to increase the uniformity of the energy absorption. To better understand the effect of this operation, we have simulated the distribution of the absorbed energy along a vertical wall at an increasing number of repositionings of a radiating source held at a fixed distance from the wall. The results in Figure 5 present how the level of homogeneity of energy absorption depends on the number of repositionings and on the distance of the lamp from the wall. The peaks can be clearly observed in correspondence to the fixed positions of the lamp [Figure 5(a)] while an almost flat profile with some boundary effects is achieved in the case of a moving source, obtaining an optimal distribution of the irradiated energy along all of the surface. Correspondingly, in Figure 5(b) the simulation demonstrates how the required exposure time increases if the same minimum level of irradiation energy is requested. In particular, when the geometry of a room, i.e., a rectangular or any asymmetrically shaped room (such as a corridor), or obstacles within a room constrain the robot to be close to the surface, the time required by a fixed lamp must be a multiple of the time required by a moving one. If we consider the cost of the manpower needed to reposition the source, overall disinfection costs are then multiplied by a higher value.

After 30 min of exposure, log-3 SARS-CoV-2 virus inactivation values (3.7 mJ/cm^2) were reached by 100% of the samples in the dynamic condition.

A Motion-Planning Algorithm Based on Irradiation Physics

Overview

This first study demonstrated how robots can improve disinfection accuracy and reduce task-execution time by moving the radiation source, thus distributing energy more homogeneously in the environment. The disinfection problem can be seen as a special case of motion planning and navigation in dynamic environments, where the mission target is composed of a large number of variable target points, i.e., all of the

Color					
Green Value (RGB)	248	181.2	174.7	141.1	117.7
Energy (mJ/cm^2)	0	25	50	75	100

Figure 4. The reference chart provided by the manufacturer for the energy–density calculation from the G channel of the marker's color.

Table 1. The paired t-test of a UV-irradiation average dose, * $p < 0.05$.

Time	Mean	Standard Deviation	*p* Value
6 min	3.22	15.09	Not significant
12 min	7.22	23.66	Not significant
18 min	10.84	27.98	$p = 0.091$
24 min	13.21*	28.42*	$p < 0.05$
30 min	13.21	30.45	$p = 0.061$

The disinfection problem can be seen as a special case of motion planning and navigation in dynamic environments.

surfaces in the environment to be disinfected by exposure to the radiating energy. Each surface should receive at least a certain minimum sufficient radiation dose, i.e., 16.9 mJ/cm^2 [8], which is dependent on both the exposure time and distance from the radiation source. Since the radiation dose received by each surface in the environment strictly depends on time, the problem must be formulated requiring that path planning and trajectory generation are coupled and simultaneously solved. Therefore, a specific approach to the problem formulation and solution needs to be devised.

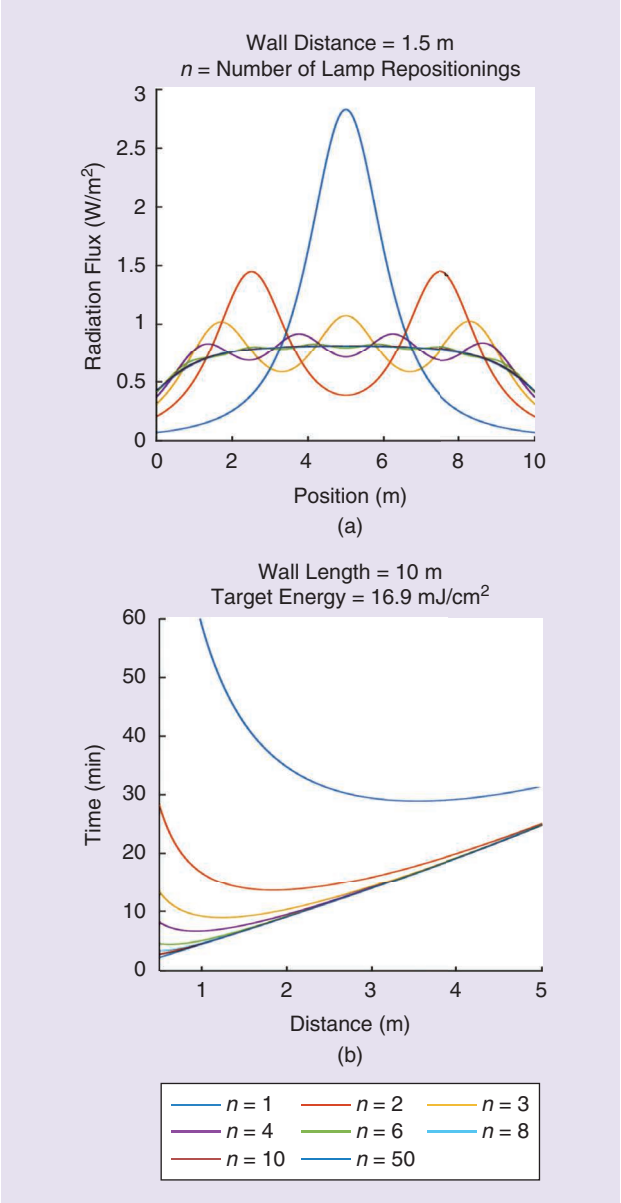

Figure 5. The simulation of (a) the radiation energy absorbed along a vertical surface at an increasing number of repositionings of a static UV-C lamp and (b) the time required to obtain a minimum absorbed energy of 16.9 mJ/cm^2 at any point on a 10-m vertical wall, at varying distances from the radiation source.

Navigation of mobile robots has already been deeply treated in the literature. Some of the proposed approaches where path planning and trajectory generation are solved simultaneously include APFs [14], harmonic potential functions [15], and navigation functions [16]. It has been thought that all of the previous methods have ensured that the robot can reach a given navigation goal without getting stuck into a local minimum of the potential function, yet they are not sufficient in their original formulation to solve the required disinfection motion-planning strategy. To this aim, in this article, we propose a novel motion planner and trajectory-generator algorithm specifically for disinfection procedures, based on the following three modules:

1) The first module is based on a time-varying APF that determines the robot velocity and guides it toward the surfaces to disinfect, depending on both the distance from the surfaces and the amount of energy already stored in them. The APF value is constantly modulated by the output of a second module.
2) The second module consists of a physical simulation of irradiation physics and robot motion in the environment, where the APF and amount of energy delivered to the surfaces are computed accordingly over time.
3) Module three consists of an automatic optimization method to explore different possible solutions and to optimize the process based on a GA.

The generation of a suitable disinfection trajectory for a robot is not a straightforward task; there could be many valid alternative strategies that solve the problem. In this trajectory planner, we rely on the principle that, based on irradiation physics, the closer the robot gets to a surface to disinfect, the faster this surface will be disinfected. For this reason, an APF is defined in such a way that attracts the robot toward all of the surfaces that still need disinfection. A simulation of the environment, considering both irradiation physics and robot motion, calculates the amount of energy delivered to each surface and, then, accordingly computes the APF governing the robot motion. The output of the simulation is only a possible disinfection trajectory if the complete disinfection target is achieved. Otherwise, the simulation provides a negative outcome. As many possible trajectories could be explored, the APF has coefficients that can be adjusted to change the robot motion in a substantial way. Within this framework, the role of the GA is to explore all of the different possible values of these coefficients to obtain the best feasible disinfection trajectory. Of course, the problem is strongly dependent on the target environment's geometry; the environment's shape and extension, together with the arrangement and concentration of

obstacles, affect the APF in a significant way. Because of the high computational cost, the proposed trajectory planner was not implemented in real time; based on the environment map, offline computation was performed to plan the robot motion in advance.

Irradiation Model

Here, we present the equations governing the irradiation model used by the simulation module of the trajectory planner. Let us consider the problem described in Figure 6 involving a lamp of power P mounted on the robot, which can be modeled as a light source homogeneously distributed along a vertical line of length L. We define point A as the midpoint of the lamp installed on the robot and point B as a generic point of the lamp located at a distance l from A, along the lamp. The goal is to calculate the irradiation intensity on a generic infinitesimal surface dA, with normal $\hat{n}$, located at point C. Noting that $x_B = x_A$, $y_B = y_A$, and $z_B = z_A + l$, we can write that $\vec{r} = [x_C - x_A, y_C - y_A, z_C - z_A - l]$, and we can calculate the irradiation intensity I on the surface dA as

$$I(\vec{r}, \hat{n}) = \frac{P}{4\pi L} \int_{-\frac{L}{2}}^{\frac{L}{2}} \frac{\eta(\vec{r}, \hat{n})}{|\vec{r}|^2} dl, \tag{1}$$

where η is the optical efficiency, and it is given by

$$\eta(\vec{r}, \hat{n}) = \begin{cases} \dfrac{|\vec{r} \cdot \hat{n}|}{|\vec{r}|} & \vec{r} \cdot \hat{n} \leq 0 \\ 0 & \vec{r} \cdot \hat{n} > 0 \end{cases}, \tag{2}$$

which also considers that the surface can actually be irradiated only by one side. We can calculate the energy stored in the surface by integrating the function $I(\vec{r}(t), \hat{n})$ over time.

APF

Let us suppose that a real environment can be modeled using 3D discrete surfaces that generate an attractive potential on the robot that is dependent on the distance from the robot. Since the robot can move only on the floor in a 2D environment, if there are more surfaces at the same position (x, y) with different heights (z), e.g., a wall, only the surface with the worst optical efficiency is considered in the computation of the potential. This is to avoid an unbalanced concentration of attractive charges at some coordinates. Let us denote the 2D vector as $\vec{r}_i$, which goes from the robot to the surface. The attractive potential at the robot's location is defined as

$$U(\vec{r}_i, t) = -k \sum_i w_i(t) \frac{1}{|\vec{r}_i|^n}, \tag{3}$$

where k is a constant that sets the overall magnitude of the potential, n is a constant exponent that determines the influence of the distance, and $w_i(t)$ is the surface weight. If $E_i(t)$ is the energy density already stored in the surface and E_0 is the energy density needed to complete surface disinfection, the surface weight is defined as

$$w_i(t) = \begin{cases} 1 + m\dfrac{E_i(t)}{E_0} & E_i(t) < E_0 \\ 0 & E_i(t) \geq E_0 \end{cases}, \tag{4}$$

where m is a coefficient that sets the maximum possible value of the surface weight. The surface weight has two goals: 1) it aims at preventing the robot from moving away from a surface without having completely disinfected it, and, 2) most importantly, when the surface has been completely disinfected $[E_i(t) \geq E_0]$, the surface weight is null so that the surface does not contribute any more to the total potential energy. This feature makes the APF change over time, according to the outcome of disinfection over time. The gradient of the potential function defines the velocity field in the map, considering the sum of the contributions of all of the surfaces left to disinfect, which can be written as

The role of the GA is to explore all of the different possible values of these coefficients to obtain the best feasible disinfection trajectory.

$$\vec{v} = \sum_i -\nabla U_i = \sum_i knw_i(t) \frac{\vec{r}_i}{|\vec{r}_i|^{-(n+2)}}. \tag{5}$$

However, for safety reasons, robot speed is limited to 0.2 m/s. In fact, robot dynamics are not modeled, and the speed could be unbounded, with acceleration and deceleration that are not achievable by the robot. It is important to observe that the APF alone would not be sufficient to generate suitable trajectories; in fact, it does not handle the presence of obstacles and the environment's boundaries. For this reason, each time the robot tries to trespass the environment or an obstacle's

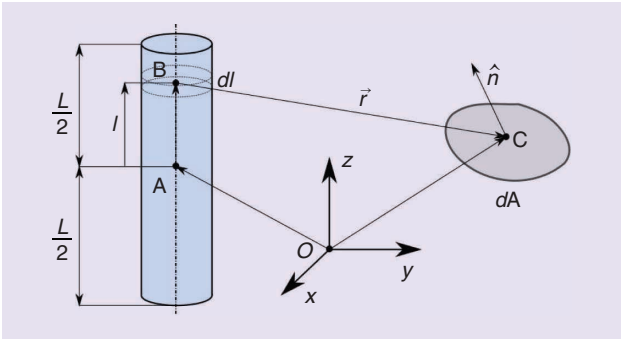

Figure 6. The irradiation model.

boundary, the velocity is modified such that it has the same magnitude but its component normal to the boundary is null. In other words, the robot is constrained to sliding along the closest obstacle boundary. If this is not possible, a random suitable velocity is assigned to the robot. Finally, it is important to note that the three coefficients (k, n, m) have a fundamental role as they can drastically change the shape of the velocity field governing the robot's motion.

It can be observed how the APF output velocity is successfully modified to allow the robot to maneuver around the obstacles and go toward the surfaces to disinfect.

Irradiation and Motion Simulation

Given the model of the environment and its surfaces, we could exploit the irradiation model described in the "Irradiation Model" section to reproduce the evolution over time, using a discrete time step of the energy density delivered by the robot during its motion. The simulation involves the execution of the following instructions at each time step:

1) It involves computing the irradiation function and updating surfaces' energy.
2) It also involves computing the velocity field in the actual robot position.
3) If $E_i \geq E_0$ for all of the surfaces in the environment, the disinfection is completed. Otherwise, the actual time value is increased by the time-step value, and the instructions are repeated starting from point 1.

The output of the simulation is the robot trajectory, generated as a sequence of coordinates over time that the robot should track during the disinfection task. As stated in the previous "Overview" and "APF" sections, different outcomes are possible by changing the APF coefficients. The irradiation and motion simulations allow us to verify whether a particular set of coefficients generates a trajectory suitable for the disinfection of the environment and to calculate the total time needed to perform the task. At this point, what is missing is a method to explore different possible choices of the APF coefficients; this part is played by the GA.

Table 2. The simulation and GA settings.

Parameter	Value	Parameter	Value
Space discretization	0.3 m	Time step	0.5 s
Population size	30	Maximum generation	300
Function tolerance	10^{-7}	Survivors	6
Selection function	Tournament, 4 m	Crossover function	Intermediate
Crossover fraction	0.5	Mutation function	Gaussian
Subsample period	2 s	Initial k	*logsp*(1e-2, 1e4)
Initial n	*linsp*(1,3)	Initial m	*linsp*(0,20)

GA

The GA has been chosen as the method to automatically explore the different possible trajectories that can be obtained using the proposed APF. This choice is motivated by the capability of the GA to explore the solution space in a stochastic way, allowing for variable values also outside of the starting range. Therefore, the three coefficients (k, n, m) are chosen as the genes of a given individual in the population while the cost function for the optimization is the total time needed for the disinfection task. We used MATLAB to run the GA, with the settings reported in Table 2. Once the optimized values are obtained, they are employed to run a final simulation that produces a raw optimized trajectory. The raw optimized trajectory is then subsampled to obtain a new, smoother one. The subsampling process is automatic and iterative: deleted points are substituted by new ones obtained from linear interpolation on the points remaining. This new trajectory is checked again through simulation to verify whether the process had compromised the effectiveness of disinfection. In case of failure, the procedure is repeated with a decreased subsampling period until a positive outcome is obtained.

Simulated Case Studies

The trajectory planner has been tested in different case studies, two significant ones among which we report (Figure 7). The first is a simple, convex environment with two square obstacles inside while the second is a nonconvex, H-shaped environment with four circular obstacles. Importantly, the trajectory planner could converge to a suitable solution, complying with the complete disinfection constraint, for several different values of the coefficients (k, n, m) in both cases and, thus, could choose the best solution in terms of time from a wide range of trajectories. Moreover, especially in the second case study, it can be observed how the APF output velocity is successfully modified to allow the robot to maneuver around the obstacles and go toward the surfaces to disinfect. Finally, we summarize the whole trajectory generation process in the flowchart in Figure 8.

Algorithm Evaluation Experiment

The goal of the second experiment was to evaluate the disinfection performance of the optimized trajectory-planning method described in the previous section. To this end, we used a meeting room [dimensions 8.6×5.6 m (2D

map and pictures in Figure 9)] in which the robot could have fewer constraints in movements compared to the room described in the first experiment. Therefore, the algorithm could choose among a wide variety of trajectories, and so it was possible to evaluate its capability of independently optimizing the path and traveling speed. We expected that the algorithm ensured the disinfection of all of the surfaces in the room and that the markers' energy distribution had a lower standard deviation compared to a "standard" trajectory.

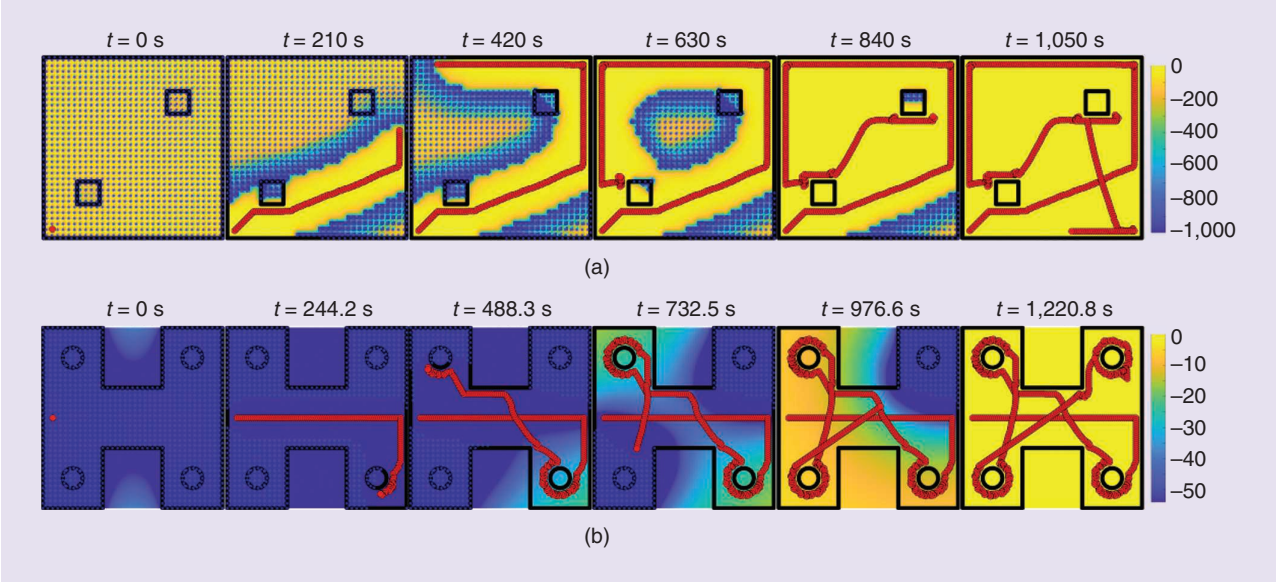

Figure 7. The trajectory planner outcomes for two different environments. The potential function value is given by the color, according to the color bar on the right. The robot's trajectory is described by the red markers' sequence; black lines represent the environment's boundaries or obstacles within the environment. (a) An 8×8-m, square-shaped environment with two tables ($k = 0.13$, $n = 2.62$, $m = 19.81$). (b) A nonconvex, H-shaped environment, 9×9 m, with four circular tables ($k = 0.32$, $n = 1.55$, $m = 10.26$).

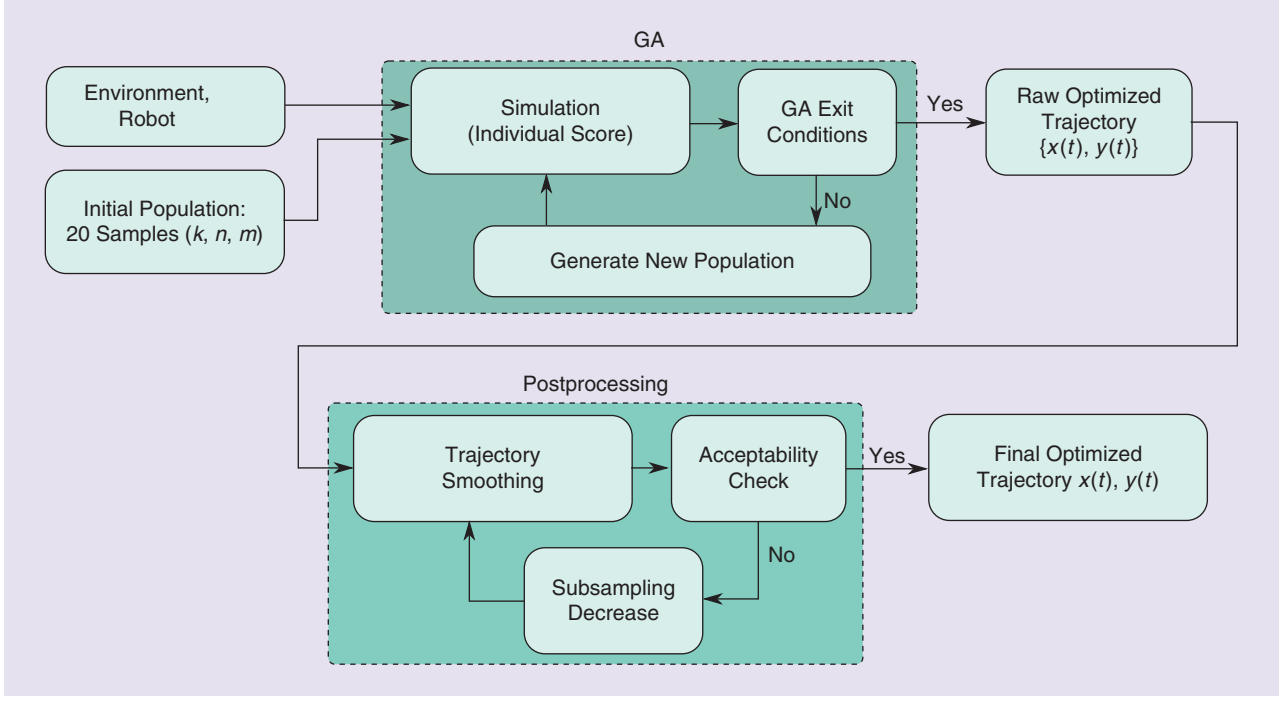

Figure 8. The optimization flow chart. Given the robot, environment data, and an initial population of the three motion-strategy parameters, the GA searches for the best values by performing a simulation for each individual in the population. When the criteria for exiting the GA are satisfied, the disinfection simulation is performed again using the optimal values, and a raw trajectory is obtained and postprocessed to generate the optimized trajectory.

Methods

The room was instrumented with 24 colorimetric UV-C-sensitive markers with different positions and orientations, located on tables (1–4), on shelves (5–9, 11, 14, 22), on walls (10, 12), on the door (13), and on the floor (15–21, 23, 24) (see Figure 9), and then it was exposed to UV-C irradiation. To have a benchmark for evaluating the algorithm performance, it was necessary to define a comparative trajectory that ensured good coverage of the room area and, thus, offered a fair comparison. We then chose the simplest trajectory allowing the robot to move across the room at a constant distance from the objects to disinfect (we call it the "standard" trajectory), and the result is the path displayed in Figure 9(a), traveled at a constant speed. Then, we performed the irradiation experiment in two different conditions: 1) the "standard" trajectory and b) a GA-optimized trajectory. The experimental comparison was carried out with equal total irradiation time for the two conditions (resulting also in equal total energy irradiated in the room). For this reason, we calculated the speed for the "standard" trajectory to match the total time needed for the GA-optimized trajectory: 594 seconds. The energy data were evaluated with the same method described in the previous "Methods" section.

Shared environments, such as conference rooms, public spaces, or workplaces, could benefit from robotic disinfection in terms of task accuracy, cost, and execution time.

Results

Figure 9 displays the results of the experiments in the two different conditions. The bar plot of the markers' energy–density distributions shows that, in the "standard" condition, only 18/24 markers were successfully disinfected (energy density > 16.9 mJ/cm^2) while, in the GA condition, the score was 24/24 (Fisher exact test $p = 0.022$). Although the average delivered energy in the GA condition is higher than in the "standard" condition and the standard deviation is lower in the GA condition than in the "standard" condition, the number of samples was not high enough to achieve a statically significant difference between the two conditions. Numerical results are reported in Table 3.

Discussion and Conclusions

This article presents 1) the performance evaluation of a UV-C-disinfection mobile robot, compared to conventional disinfection based on static UV-C lamps, and 2) the evaluation of a new trajectory-planning strategy specifically for disinfection robots. The evaluation was performed using UV-C-sensitive colorimetric detectors to measure the effective amount of absorbed energy; then data were elaborated to assess statistical significance. The static versus dynamic experiment results demonstrate that, in a wide environment, it is possible to improve the effectiveness and reduce the time of the disinfection by using a mobile source of UV-C irradiation. A significant statistical difference on the number of disinfected markers was achieved, which is the most important goal of the disinfection task.

However, this on-field experience highlights the importance of rearranging an environment to make it suitable for robotic disinfection. The robot could not reach and disinfect some areas of the room because they were too distant or not sufficiently exposed. To improve the effectiveness of robot disinfection, environments should be adequately prepared. There should not be narrow passages or obstacles left on the floor, and the most likely contaminated objects or surfaces, such as handles, tools, and desks, should be directly exposed to radiations.

Disinfection is a repetitive, frequent, and time-consuming task, and, given the demonstrated importance of a mobile source of radiation, the development of mobile robotic platforms for disinfection is a straightforward solution. It can, alone, have a significant impact on the effectiveness, time, and resources needed for the disinfection procedure.

Still, the potential of a mobile robotic platform can go further than the movement of the source of UV-C radiation. It allows the development of optimized trajectories that, although more complex, can be followed with the same accuracy and repeatability. We explored this opportunity by developing a novel trajectory planner specific for the disinfection task based on an APF, an iterative simulation method based on irradiation physics, and optimization through GA to find the most suitable trajectory. The trajectory planner has been tested in simulation, where it could produce a suitable solution ensuring the completion of disinfection for different test environments.

Still, improvements are needed to address cluttered and complex environments, where the method could suffer from the presence of multiple obstacles or nonconvex boundaries. These environments can be addressed by dividing them into suitable subenvironments that can be handled by the proposed trajectory planner and by using high-level logic to switch from one subenvironment to another.

Finally, by means of our UV-C mobile robot, we experimented on the effectiveness of the trajectory planner in a real setting. Results, again, confirmed the importance of carefully choosing the trajectory to minimize the time needed for disinfection. The proposed model scored a 100% disinfection success rate (24/24 markers) against the 75% of the benchmark "standard" trajectory; the benchmark trajectory requires more time for completing the disinfection on all of the surfaces in the environment.

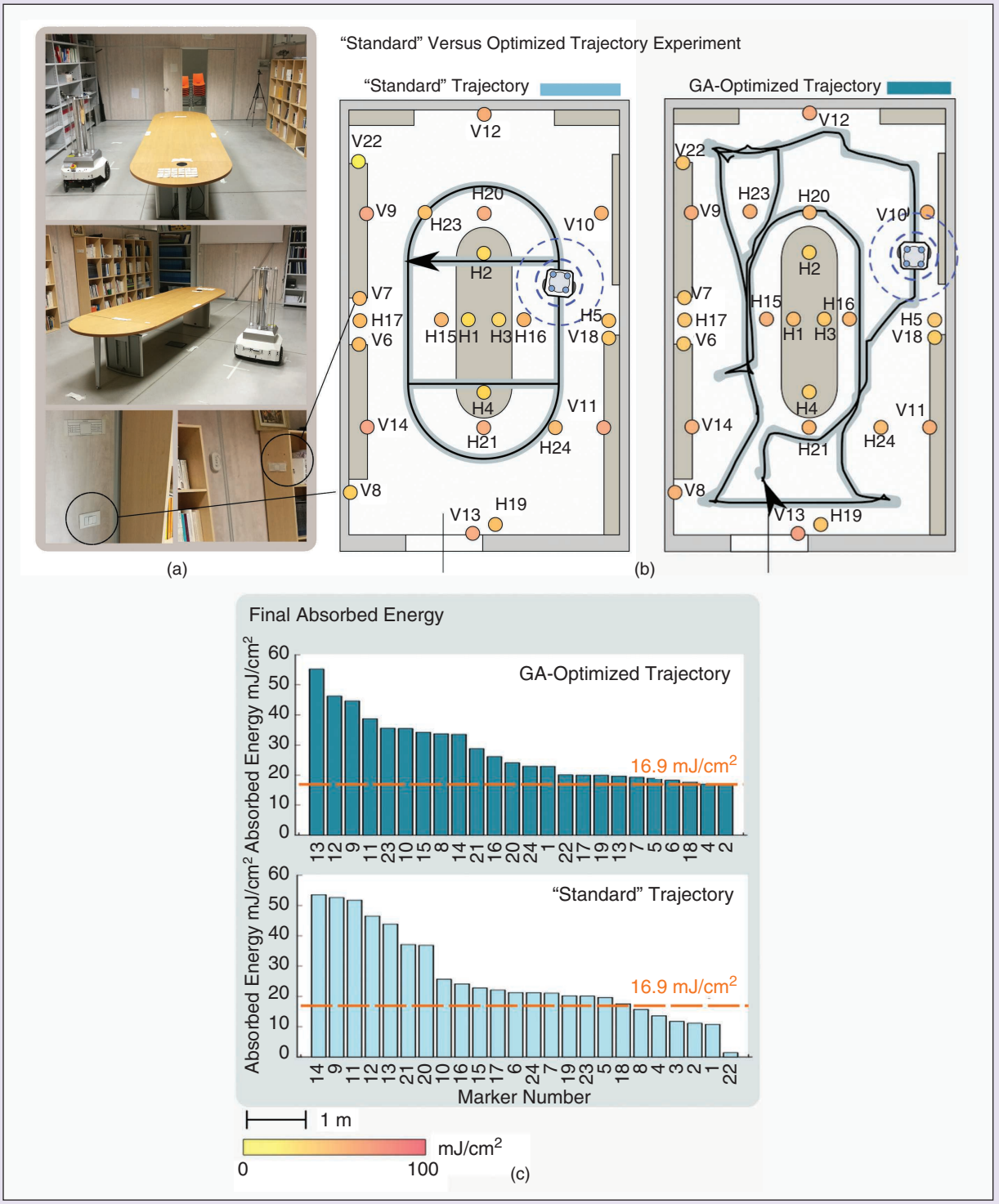

Figure 9. The results of the GA evaluation experiment. (a) The experimental setup. (b) Maps of the two experiments, which report the desired trajectory (shaded gray) and robot's actual trajectory (black) and the markers' positions and colors at the end of the experiment. The marker's code starts with "H" if it is horizontal (e.g., if it lies on the floor) or "V" if it is vertical (e.g., if it is attached on the wall). (c) Bar plots of the energy–density distribution in the two different conditions.

Table 3. The GA evaluation experiment results, *$p < 0.05$.

Experiment	Disinfection Markers	Mean Energy	Standard Deviation
Standard	18/24*	25.93 mJ/cm^2	14.63 mJ/cm^2
GA-optimized	24/24*	27.93 mJ/cm^2	10.67 mJ/cm^2

On the other hand, no significant results were achieved in terms of the mean or variance of the energy–density distributions in the two conditions. A possible explanation for this is the relatively low number of markers used to assess these variables. However, these results encourage the use of disinfection robots as a valid alternative to traditional disinfection methods. Shared environments, such as conference rooms, public spaces, or workplaces, could benefit from robotic disinfection in terms of task accuracy, cost, and execution time. This example of robotic application in this period of emergency strongly supports the idea that the knowledge and experience of the robotic community can be crucial in the fight against COVID-19 and in the limitations the virus is imposing on us and our lifestyle.

References

[1] G.-Z. Yang et al., "Combating COVID-19–the role of robotics in managing public health and infectious diseases," *Sci. Robot.*, vol. 5, no. 40, p. eabb5589, 2020. doi: 10.1126/scirobotics.abb5589.

[2] M. Tavakoli, J. Carriere, and A. Torabi, "Robotics, smart wearable technologies, and autonomous intelligent systems for healthcare during the COVID-19 pandemic: An analysis of the state of the art and future vision," *Adv. Intell. Syst.*, vol. 2, no. 7, p. 2,000,071, 2020. doi: 10.1002/aisy.202000071.

[3] Q. C. Feng and X. Wang, "Design of disinfection robot for livestock breeding," *Procedia Comput. Sci.*, vol. 166, pp. 310–314, 2020. [Online]. Available: https://www.sciencedirect.com/science/article/pii/S1877050920302155 doi: 10.1016/j.procs.2020.02.093.

[4] J. Otter, S. Yezli, T. M. Perl, F. Barbut, and G. French, "The role of 'no-touch' automated room disinfection systems in infection prevention and control," *J. Hosp. Infect.*, vol. 83, no. 1, pp. 1–13, 2013. doi: 10.1016/j.jhin.2012.10.002.

[5] A. Begić, "Application of service robots for disinfection in medical institutions," in *Proc. Int. Symp. Innov. Interdisciplinary Appl. Adv. Technol.*, 2017, pp. 1056–1065. doi: 10.1007/978-3-319-71321-2_89.

[6] B. Casini et al., "Evaluation of an ultraviolet c (UVC) light-emitting device for disinfection of high touch surfaces in hospital critical areas," *Int. J. Environ. Res. Public Health*, vol. 16, no. 19, p. 3572, 2019. doi: 10.3390/ijerph16193572.

[7] M. Nottingham et al., "Ultraviolet-C light as a means of disinfecting anesthesia workstations," *Amer. J. Infect. Control*, vol. 45, no. 9, pp. 1011–1013, 2017. doi: 10.1016/j.ajic.2017.02.016.

[8] A. Bianco et al., "UV-C irradiation is highly effective in inactivating and inhibiting SARS-CoV-2 replication," 2020. [Online]. Available: https://papers.ssrn.com/sol3/papers.cfm?abstract_id=3620830

[9] J.-H. Yang, U.-I. Wu, H.-M. Tai, and W.-H. Sheng, "Effectiveness of an ultraviolet-c disinfection system for reduction of healthcare-associated pathogens," *J. Microbiol. Immunol. Infect.*, vol. 52, no. 3, pp. 487–493, 2019. doi: 10.1016/j.jmii.2017.08.017.

[10] P. Chanprakon, T. Sae-Oung, T. Treebupachatsakul, P. Hannanta-Anan, and W. Piyawattanametha, "An ultra-violet sterilization robot for disinfection," in *Proc. 2019 5th Int. Conf. Eng. Appl. Sci. Technol. (ICEAST)*, pp. 1–4. doi: 10.1109/ICEAST.2019.8802528.

[11] M. Labbé and F. Michaud, "RTAB-map as an open-source lidar and visual simultaneous localization and mapping library for large-scale and long-term online operation," *J. Field Robot.*, vol. 36, no. 2, pp. 416–446, 2019. doi: 10.1002/rob.21831.

[12] C. Liscynesky, L. P. Hines, J. Smyer, M. Hanrahan, R. C. Orellana, and J. E. Mangino, "The effect of ultraviolet light on *Clostridium difficile* spore recovery versus bleach alone," *Infect. Control Hosp. Epidemiol.*, vol. 38, no. 9, pp. 1116–1117, 2017. doi: 10.1017/ice.2017.126.

[13] T. Wong et al., "Postdischarge decontamination of MRSA, VRE, and *Clostridium difficile* isolation rooms using 2 commercially available automated ultraviolet-C–emitting devices," *Amer. J. Infect. Control*, vol. 44, no. 4, pp. 416–420, 2016. doi: 10.1016/j.ajic.2015.10.016.

[14] O. Khatib, "Real-time obstacle avoidance for manipulators and mobile robots," in *Autonomous Robot Vehicles*, New York: Springer-Verlag, 1986, pp. 396–404.

[15] C. I. Connolly, J. B. Burns, and R. Weiss, "Path planning using Laplace's equation," in *Proc. IEEE Int. Conf. Robot. Automat.*, 1990, pp. 2102–2106. doi: 10.1109/ROBOT.1990.126315.

[16] C. Chen, C. Li, and H. G. Tanner, "Navigation functions with non-point destinations and moving obstacle," in *Proc. 2020 Amer. Control Conf. (ACC)*, 2020, pp. 2532–2537. doi: 10.23919/ACC45564.2020.9147243.

Luca Tiseni, Percro Laboratory, Tecip Institute, Sant'Anna School of Advanced Studies, Pisa, 56010, Italy. Email: luca.tiseni@santannapisa.it.

Domenico Chiaradia, Percro Laboratory, Tecip Institute, Sant'Anna School of Advanced Studies, Pisa, 56010, Italy. Email: domenico.chiaradia@santannapisa.it.

Massimiliano Gabardi, Percro Laboratory, Tecip Institute, Sant'Anna School of Advanced Studies, 56010, Pisa, Italy. Email: massimiliano.gabardi@santannapisa.it.

Massimiliano Solazzi, Percro Laboratory, Tecip Institute, Sant'Anna School of Advanced Studies, Pisa, 56010, Italy. Email: massimiliano.solazzi@santannapisa.it.

Daniele Leonardis, Percro Laboratory, Tecip Institute, Sant'Anna School of Advanced Studies, Pisa, 56010, Italy. Email: daniele.leonardis@santannapisa.it.

Antonio Frisoli, Percro Laboratory, Tecip Institute, Sant'Anna School of Advanced Studies, Pisa, 56010, Italy. Email: antonio.frisoli@santannapisa.it.